

Inference of stochastic time series with missing data

Sangwon Lee,¹ Vipul Periwal,^{2,*} and Junghyo Jo^{3,4,†}

¹*Department of Physics and Astronomy, Seoul National University, Seoul 08826, Korea*

²*Laboratory of Biological Modeling, National Institute of Diabetes and Digestive and Kidney Diseases, National Institutes of Health, Bethesda, Maryland 20892, USA*

³*Department of Physics Education and Center for Theoretical Physics and Artificial Intelligence Institute, Seoul National University, Seoul 08826, Korea*

⁴*School of Computational Sciences, Korea Institute for Advanced Study, Seoul 02455, Korea*

(Dated: February 28, 2025)

Inferring dynamics from time series is an important objective in data analysis. In particular, it is challenging to infer stochastic dynamics given incomplete data. We propose an expectation maximization (EM) algorithm that iterates between alternating two steps: E-step restores missing data points, while M-step infers an underlying network model of restored data. Using synthetic data generated by a kinetic Ising model, we confirm that the algorithm works for restoring missing data points as well as inferring the underlying model. At the initial iteration of the EM algorithm, the model inference shows better model-data consistency with observed data points than with missing data points. As we keep iterating, however, missing data points show better model-data consistency. We find that demanding equal consistency of observed and missing data points provides an effective stopping criterion for the iteration to prevent overshooting the most accurate model inference. Armed with this EM algorithm with this stopping criterion, we infer missing data points and an underlying network from a time-series data of real neuronal activities. Our method recovers collective properties of neuronal activities, such as time correlations and firing statistics, which have previously never been optimized to fit.

I. INTRODUCTION

System identification is one of the most important tasks in data science [1]. To be specific, suppose we have observations $\{\vec{\sigma}(t)\}$ of a sample $\vec{\sigma} = (\sigma_1, \sigma_2, \dots, \sigma_N)$, where t can denote a time index for time series data, or a sample index for independent data. Considering stochastic systems, statistical mechanics has been adopted to construct the least structured probabilistic model of $P(\vec{\sigma})$ from observations. In particular, Ising-like models of $P(\vec{\sigma}) \propto \exp(\sum_{i,j} W_{ij} \sigma_i \sigma_j)$ incorporate the pair-wise interactions between variables. Its applicability ranges from neuroscience and biology [2–7] to economics and sociology [8–10]. Such pairwise interactions are sufficient to explain complex higher-order patterns in many cases [2, 11], and the efficacy and limitations of these models have also been extensively studied [12]. To consider time-dependent data arising from kinetic interactions, another type of Ising model has been proposed [13]. Unlike the equilibrium model of $P(\vec{\sigma})$, the kinetic Ising model has a probabilistic relation between $\sigma_i(t+1)$ and $\sigma_j(t)$ with the conditional probability of $P(\sigma_i(t+1)|\vec{\sigma}(t)) \propto \exp(\sum_j W_{ij} \sigma_i(t+1) \sigma_j(t))$. The kinetic model has been used to reconstruct neural networks from temporal neuronal activities [14, 15].

Both equilibrium and kinetic (or non-equilibrium) models have network parameters W_{ij} . In the equilibrium model, it is symmetric ($W_{ij} = W_{ji}$) to represent undirected correlation between σ_i and σ_j . However,

in the kinetic model, W_{ij} is not necessarily symmetric ($W_{ij} \neq W_{ji}$) as it represents directed causality from $\sigma_j(t)$ to $\sigma_i(t+1)$. Due to the wide applications of these models, it is an important inverse problem to infer W_{ij} from observations $\{\vec{\sigma}(t)\}$. As concretely established in the equilibrium model [16], the kinetic model also has many inference methods including various mean-field approximations [14, 17], maximum likelihood estimation [14, 15], and the recent expectation-reflection method [18].

In real-world problems, it is common that only a part of a network is observable. For example, it is impossible to observe every neuron in the brain. Therefore, one should consider not only observed visible units but also unobserved hidden units. Much effort has been devoted to infer both hidden variables and the network parameters [19–23]. These methods basically rely on the celebrated expectation maximization (EM) algorithm [24]. The EM method is composed of two iterative steps: E-step predicts hidden variables by using mean-field approaches [19, 20], replica methods [21, 22], or a likelihood-based method [23], and M-step optimizes the network parameters from the reconstructed data.

In addition to the issue of hidden units, another practical issue is that even visible units are not always observable throughout an experiment. At each time point, some units become accessible to observers and the others become inaccessible. For example, a large-scale neural network can be partially scannable in neuroscience experiments [25]. This scenario is also common in finance and social science [26]. For a trading network, trade records are available only when traders are active. Although some remarkable works exist, the research on the kinetic Ising model with missing or partially masked

* Corresponding author: vipulp@mail.nih.gov

† Corresponding author: jojunghyo@snu.ac.kr

data is still in its infancy. Camajola *et al.* [26] addressed this issue inspired by the mean-field approach of Dunn *et al.* [19] that was originally developed to address the issue of hidden units. The mean-field approach imposes an a priori assumption that interactions are weak and dense [20]. Thus it is imperative to develop an approach free from such constraints. Of course, any such method has to be tested against real-world problems beyond the proof-of-concept with synthetic data.

Here we develop a general method to infer the parameters of a kinetic Ising model from data with sporadic missing values of any measured variable, extending our recent study on hidden variables [23]. The algorithm uses the EM method: the E-step restores missing time points stochastically using a likelihood ratio, while the M-step infers network parameters from observed and restored data. Alternation of these two steps infers network coupling parameters as we iterate but excessive iteration finally ends up with overestimation of the parameters. It is therefore crucial to find a criterion for stopping EM iterations that can be applied to real-world data. We find that the optimal number of iterations is reached when one obtains equal inference loss for both observed and restored data. Using the EM method with the optimal number of iterations, we demonstrate that our method successfully infers synthetic data of the kinetic Ising model. We then apply the method to infer kinetics of a neuronal network from real neuronal activity data [27, 28], and confirm that the inference reproduces collective behaviors such as time correlation and firing statistics of neuronal activities.

This paper is organized as follows. In Sec. II, we describe our EM-based method and the stopping criterion for optimal iterations. In Sec. III, we validate this method with simulated data using the kinetic Ising model and examine inference performance depending on the fraction of missing observations, interaction strengths, and sample size. We then apply the method to infer dynamics from real neuronal activity data, and compare the inference performance with equilibrium and null models. Finally, we summarize and discuss our findings in Sec. IV. To keep the paper relatively self-contained, we explain the equilibrium model in Appendix A and describe additional experimental data on neuronal activities in Appendix B.

II. METHOD

We consider stochastic dynamics of the kinetic Ising model with N binary variables. The i -th spin $\sigma_i(t+1)$ at time $t+1$ is probabilistically determined by the conditional probability:

$$P(\sigma_i(t+1) = \pm 1 | \vec{\sigma}(t)) = \frac{\exp[\pm H_i(t)]}{\exp[H_i(t)] + \exp[-H_i(t)]}, \quad (1)$$

where the local field $H_i(t) = \sum_j W_{ij} \sigma_j(t) + b_i$ integrates the influence of connected spins as well as external bias

b_i . Here we choose a synchronous update for simplicity; refer to [15, 29] for an asynchronous update. Given binary time series data $\{\vec{\sigma}(t)\}_{t=1}^L$ of length L , various methods exist to infer W_{ij} in Eq. (1) [14, 16–18]. In particular, the expectation-reflection method provides faster inference than the standard maximum likelihood estimation, since the iterative algorithm is based on a multiplicative and parallelizable parameter update [23]. In this study, however, we used simply a logistic regression function included in a Python package, *scikit-learn* [30], because the logistic regression shows similar performance with the expectation-reflection method with high accuracy and fast computation. Note that Eq. (1) implies the logistic function:

$$P(\sigma_i(t+1) = 1 | \vec{\sigma}(t)) = \frac{1}{1 + \exp[-2 \sum_j W_{ij} \sigma_j(t) - 2b_i]}. \quad (2)$$

Now suppose that some of the data points are missing. Let \mathcal{M} denote the set of missing data values. To recover these missing values, we first assign random binary values for $\sigma_i(t)$ at every $(i, t) \in \mathcal{M}$. Then, from the observed and the randomly-assigned values of $\{\vec{\sigma}(t)\}_{t=1}^L$, we can infer a first approximation to W_{ij} using the logistic regression in Eq. (2). Next, we define a likelihood function for $\sigma_i(t) = \pm 1$ ($t \neq 1$ or L) as

$$\mathcal{L}_{i,t}^{\pm} = P(\sigma_i(t) = \pm 1 | \vec{\sigma}(t-1)) \prod_{j=1}^N P(\sigma_j(t+1) | F_i^{\pm}(\vec{\sigma}(t))), \quad (3)$$

where $F_i^{\pm}(\vec{\sigma}(t)) = (\sigma_1(t), \dots, \sigma_i(t) = \pm 1, \dots, \sigma_N(t))$. Note that $\mathcal{L}_{i,t}^{\pm}$ is a product of the likelihoods determined by the one-step backward state of $\vec{\sigma}(t-1)$ and the one-step forward state $\vec{\sigma}(t+1)$. The likelihoods for $t=1$ and L involve only forward and backward states, respectively: $\mathcal{L}_{i,1}^{\pm} = \prod_{j=1}^N P(\sigma_j(2) | F_i^{\pm}(\vec{\sigma}(1)))$ and $\mathcal{L}_{i,L}^{\pm} = P(\sigma_i(L) = \pm 1 | \vec{\sigma}(L-1))$. After defining the likelihoods, we re-assign ± 1 to $\sigma_i(t)$ with a probability of $\mathcal{L}_{i,t}^{\pm} / (\mathcal{L}_{i,t}^+ + \mathcal{L}_{i,t}^-)$ for the missing data points of $(i, t) \in \mathcal{M}$. We update the missing data points in ascending order for t and random order for i . Note that update of one missing point is affected by other missing points that may or may not have been updated in that step. After updating all the missing data points (E-step), we optimize W_{ij} from the observed and restored data (M-step). Repeating these E- and M-steps, W_{ij} is expected to converge to the true set of coupling strengths.

However, excess iteration ends up with overestimation of W_{ij} , especially when a larger fraction of data is missing. Real world problems do not come with known true W_{ij} , so how can we figure out the optimal number of iterations to maximize the goodness of fit of the inferred W_{ij} ? As a quality measure of inference, we consider the data-model consistency between $\sigma_i(t+1)$ and its expect-

tation value:

$$\begin{aligned} \langle \sigma_i(t+1) \rangle &= \sigma_i(t+1)P(\sigma_i(t+1)|\vec{\sigma}(t)) \\ &\quad - \sigma_i(t+1)[1 - P(\sigma_i(t+1)|\vec{\sigma}(t))] \\ &= \sigma_i(t+1)[2P(\sigma_i(t+1)|\vec{\sigma}(t)) - 1]. \end{aligned} \quad (4)$$

The expectation value is simply obtained as $\langle \sigma_i(t+1) \rangle = \tanh H_i(t)$ for the kinetic Ising model following the conditional probability of Eq. (1). Here the discrepancy between $\sigma_i(t+1)$ and its expectation $\langle \sigma_i(t+1) \rangle$ can be quantified as

$$\begin{aligned} D &= \sum_{i,t} [\sigma_i(t+1) - \langle \sigma_i(t+1) \rangle]^2 \\ &= \sum_{i,t} \sigma_i^2(t+1) [2 - 2P(\sigma_i(t+1)|\vec{\sigma}(t))]^2 \\ &= 4 \sum_{i,t} [1 - P(\sigma_i(t+1)|\vec{\sigma}(t))]^2 \end{aligned} \quad (5)$$

for every data point. For the derivation of the second line in Eq. (5), we used Eq. (4). Thus the discrepancy D measures the loss of the likelihood $P(\sigma_i(t+1)|\vec{\sigma}(t))$ of data $\{\vec{\sigma}(t)\}_{t=1}^L$. To separately examine the data-model consistency for observed and missing data points, we split D as $D = D_{\text{obs}} + D_{\text{mis}}$, where D_{obs} and D_{mis} represent the discrepancy contribution from observed data points ($(i,t) \notin \mathcal{M}$) and missing data points ($(i,t) \in \mathcal{M}$), respectively. During the iterations of the EM steps, both D_{obs} and D_{mis} keep decreasing because the M-step optimizes to minimize the data-model consistency. However, the relative size of two discrepancies of D_{obs} and D_{mis} changes with iterations. Therefore, the separate measures, D_{obs} and D_{mis} , can provide a good stopping criterion for the EM iterations as follows: At the beginning of the iterations, D_{mis} has a larger discrepancy because the missing data points of $\sigma_i(t)$ are randomly assigned. After some iterations, however, the missing data points are excessively fine-tuned whereas the observed data points are always fixed. This makes D_{mis} smaller than D_{obs} . Therefore, it is natural to halt the iterations when the D_{obs} and D_{mis} curves cross each other to prevent overfitting.

Finally we summarize the overall procedure:

(i) Initialize missing data $\sigma_i(t)$ for $(i,t) \in \mathcal{M}$ with random binary values;

(ii) M-step: Infer interaction parameters W_{ij} from the whole data using the logistic regression in Eq. (2);

(iii) E-step: Re-assign the missing data based on the likelihood ratio $\mathcal{L}_{i,t}^{\pm}/(\mathcal{L}_{i,t}^+ + \mathcal{L}_{i,t}^-)$ in Eq. (3);

(iv) Repeat (ii) and (iii) until $D_{\text{mis}} - D_{\text{obs}} < \epsilon$ holds with a small threshold ϵ .

III. RESULTS

We test the performance of our method with simulated data using the kinetic Ising model. After checking the concordance of inferred and true couplings with this

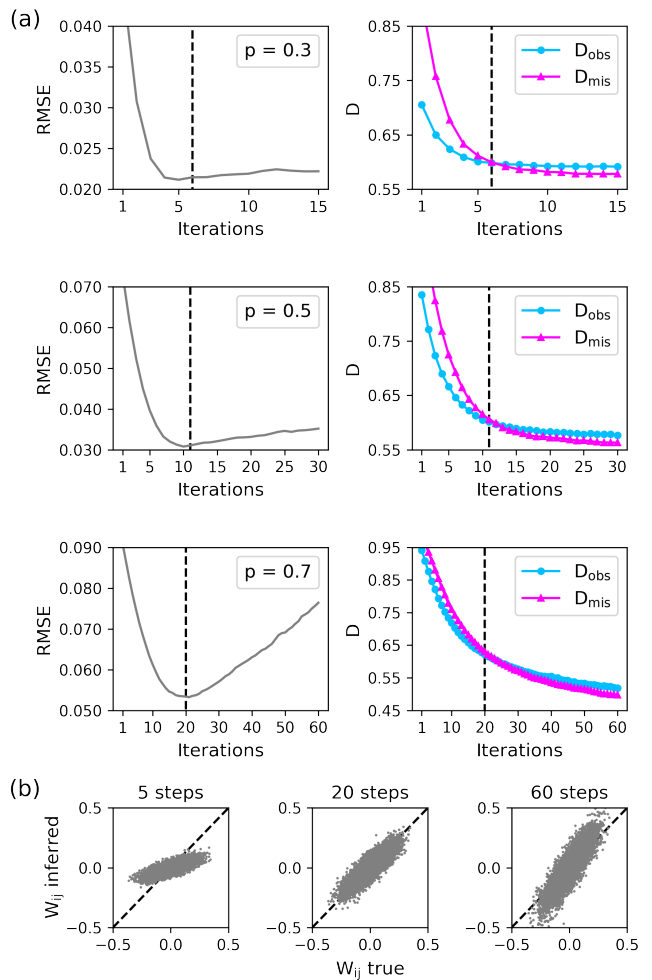


FIG. 1. (a) The evolution of root-mean-square errors (RMSE) of W_{ij} (left panels) and two quality measures of the inference, D_{obs} and D_{mis} (right panels), over the iteration of E- and M-steps. Black dotted lines denote the time when the algorithm stops according to our stopping criterion. (b) Comparison between the true and inferred W_{ij} at different times: 5 (left), 20 (center), and 60 (right) steps after the iteration starts. A fraction of missing observations was $p = 0.7$, and the correct stopping point was 20 steps according to our stopping criterion. A system size $N = 100$ and a data length $L = 10000$ was used.

simulated data, we apply the method to examine experimental recordings of neuronal activities.

A. Inference of kinetic Ising model

We simulated a stochastic time series using the Sherrington-Kirkpatrick (SK) model [31]. The SK model follows the conditional probability in Eq. (1), where the local field is defined as $H_i = \sum_j W_{ij}\sigma_j + b_i$. We turn off the bias $b_i = 0$ for simplicity, and consider asymmetric interactions $W_{ij} \neq W_{ji}$. In the SK model, each value of W_{ij} is independently drawn from a Gaussian dis-

tribution, $\mathcal{N}(0, g^2/N)$, with zero mean and the variance of g^2/N . We set the overall scale of the interaction as $g = 1$. With the selected W_{ij}^{true} , we obtain $L = 10000$ time points of $\vec{\sigma}(t) = (\sigma_1(t), \sigma_2(t), \dots, \sigma_N(t))$ with a system size of $N = 100$. Then the total number of data values of $(i, t) \in \mathcal{A}$ has a set size $|\mathcal{A}| = LN$. We then hide some data points of $(i, t) \in \mathcal{M}$ as well as the true W_{ij}^{true} . The fraction of missing data is defined as $p = |\mathcal{M}|/|\mathcal{A}|$. Our task is two folds: to restore the missing data points and to infer the true W_{ij}^{true} .

As the EM algorithm iterates, we evaluate the quality of the inference by measuring the root-mean-square error of W_{ij} , $\text{RMSE} = N^{-1} \sqrt{\sum_{i,j} (W_{ij} - W_{ij}^{\text{true}})^2}$, as in [26]. Too many iterations usually lead to increasing RMSE (Fig. 1(a)). In particular, the over-fitting becomes more evident when the fraction of missing data points increases. At early iterations, W_{ij} is underestimated because the missing data restored with random values reduce the correlation between variables (Fig. 1(b), left panels). On the other hand, at excessive iterations, W_{ij} is overestimated because the discrete values of the restored missing data are even better fitted with exaggerated H_i or larger values of W_{ij} (right panels). An optimal iteration gives an unbiased estimation of W_{ij} (center panels). Together with the RMSE, we examine the model-data consistency measures of D_{obs} and D_{mis} for the observed and missing data points. As expected, D_{mis} is larger than D_{obs} at the beginning of iterations when the restoration of missing data points is more or less random. However, after some iterations, D_{mis} becomes smaller than D_{obs} since the restoration is excessively fine-tuned. Interestingly, the equality of D_{mis} and D_{obs} occurs at the optimal iteration that minimizes the RMSE. In practice, the crossing iteration can be monitored by an inequality condition, $D_{\text{mis}} - D_{\text{obs}} < \epsilon$ with a small positive ϵ . Here we used $\epsilon = 0.01$ since smaller thresholds did not qualitatively affect the results.

After justifying the stopping criterion, we examined the performance of our inference process with varying p . Figure 2(a) is a scatter plot of the true versus inferred W_{ij} for $p = 0$ (intact data), 0.3, 0.5, and 0.7. It is evident that the inferred W_{ij} deviates farther from its true value, and the scatter plot becomes broader as the fraction of missing values, p , increases, as expected. However, the result for $p = 0.3$ is nearly indistinguishable from the one for complete data.

We then examined the collective behavior of data, particularly the one-step lagged correlation: $D_{ij} = \langle \sigma_i(t)\sigma_j(t+1) \rangle_t - \langle \sigma_i(t) \rangle_t \langle \sigma_j(t) \rangle_t$. Here $\langle f(t) \rangle_t \equiv 1/(L-1) \sum_{t=1}^{L-1} f(t)$ represents a time-averaged value of $f(t)$. Note that $\langle \sigma_j(t+1) \rangle_t \approx \langle \sigma_j(t) \rangle_t$ for large L . We compared D_{ij} computed from complete and restored data. Figure 2(b) shows that the one-step lagged correlations are successfully recovered with our inference even if a large fraction ($p = 0.7$) of data is missing.

To evaluate the quality of data restoration, we defined the restoration accuracy (RA) as the ratio of masked data

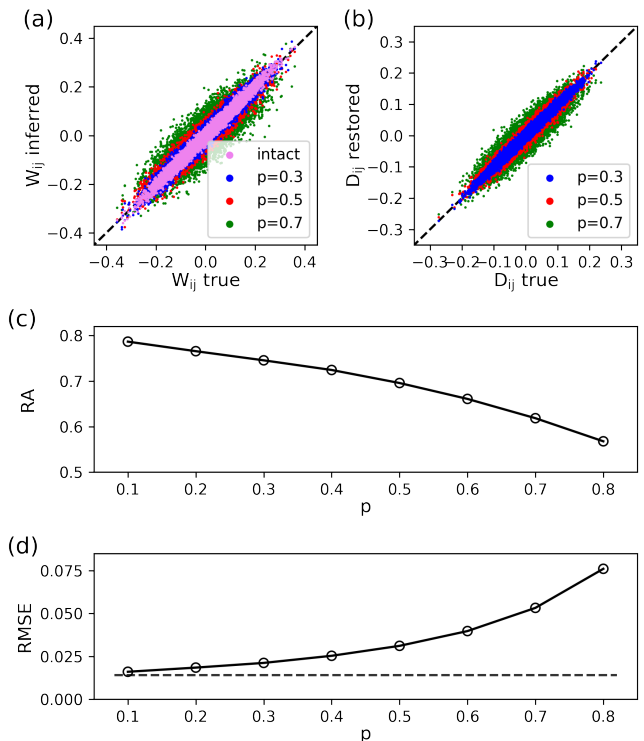


FIG. 2. Inference of coupling parameters W_{ij} and reconstruction of missing data. (a) Comparison between the true and inferred W_{ij} with a fraction of missing observations $p = 0.3$ (blue), 0.5 (red), and 0.7 (green). A result from the full data (purple) is also shown. (b) Comparison between the true and restored one-step lagged correlation D_{ij} . (c) Restoration accuracy (RA) of missing data and (d) RMSE of W_{ij} as a function of p . Black dotted line in (d) refers to the RMSE when the full data have been used. A system size $N = 100$ and a data length $L = 10000$ were used.

points that are correctly restored. Figure 2(c) shows that RA decreases with p . Specifically, when 10% of the data was missing, nearly 80% was correctly restored. However, if 80% of the data was missing, the restoration was more or less the same as a random restoration. While RA decreases with p , RMSE increases with p as Fig. 2(d). The RMSE for $p = 0.8$ becomes about 5.5 times larger than the RMSE for intact data. The RA and RMSE look comparable with the results of a mean-field approach [26], but we emphasize that our algorithm with its stopping criterion does not lead to under- or over-estimation of W_{ij} (see Fig. 2(a)). In contrast, the mean-field approach reported that when a considerable fraction of data is missing, inferred W_{ij} tends to be biased towards zero [26].

The inference performance usually depends greatly on the interaction strength g and the length L of time series. Thus we examine their dependency for the restoration and inference by varying g and L with a fixed system size $N = 80$. First, we found that RA increases as g increases (Fig. 3(a)). This is expected because strong interactions lower stochasticity in the kinetic Ising model. For a large

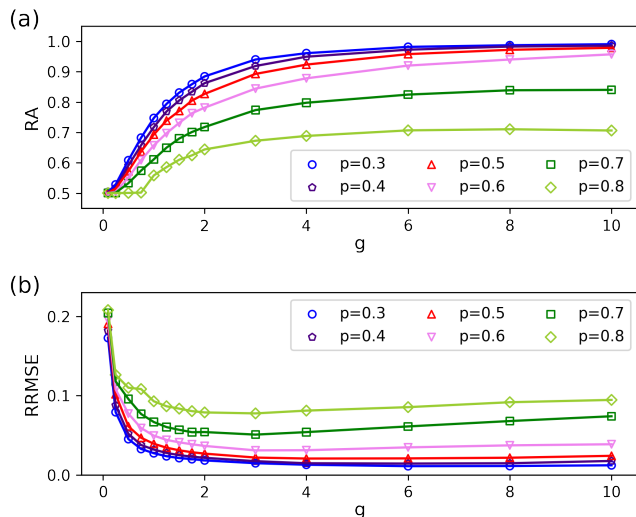


FIG. 3. (a) RA of missing data and (b) rescaled RMSE of W_{ij} as a function of the scale of couplings g from 0.1 to 10. A system size was $N = 80$ and a data length was $L = 6400$, while a fraction of missing observations p was in the range from 0.3 to 0.8.

$g \simeq 10$ and $p \leq 0.6$, almost all missing data can be correctly restored. On the other hand, when $p \geq 0.7$, the RA becomes significantly less than 1 even with large values of g . When g is too small (≤ 0.25), the binary variables have random flips resulting in RA around 50%.

Next, to address the quality of the inference of W_{ij} , we used the re-scaled RMSE defined in [26], $\text{RRMSE} = \text{RMSE}/g$. In general, RRMSE is a decreasing function of g (Fig. 3(b)). Similar to the worse restoration (Fig. 3(a)), this is because small g induces larger stochasticity with a flip probability close to 50%, which makes inference more difficult. When the fraction of missing data is small ($p \leq 0.6$), the inference shows equivalent performance with similar RRMSE values. When $p \geq 0.7$, the RRMSE becomes suddenly larger than the result of $p \leq 0.6$, especially when g is large. Taken together, these results indicate that our algorithm is applicable to a wide range of g (from 0.5 to 10) at least when p is less than 0.6.

Figure 4 shows that the quality of the inference increases with a data length L , which is not surprising. Especially from Fig. 4(b), we can observe that the error of W_{ij} follows a power-law like behavior in the wide range of L/N^2 from $1/8$ to 8, which was also detected by Campajola *et al.* [26]. We can also see that the power-law exponent does not depend on p . These results can be used to guide the appropriate sample size for applying our inference algorithm.

B. Inference of neuronal dynamics

Having confirmed that our algorithm works for synthetic data, we now apply the algorithm to explore real

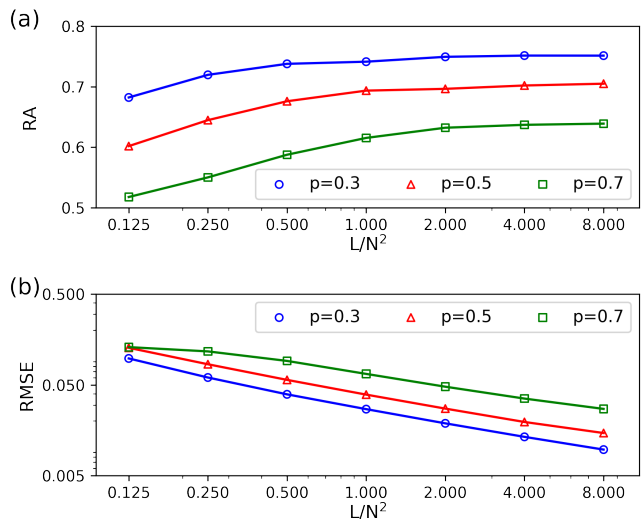


FIG. 4. (a) RA of missing data and (b) RMSE of W_{ij} as a function of L/N^2 from 0.125 to 8, where L is a data length and a system size was $N = 80$. A fraction of missing observations p was 0.3, 0.5, or 0.7.

data. We examine temporal data of neuronal activities recorded in salamander retinal ganglion cells [32]. The data consist of neuronal spike trains of 160 neurons, whose bin size is 20 ms. The state of each bin is considered *active* ($\sigma_i(t) = 1$) when at least one spike is present in the time bin, and *inactive* ($\sigma_i(t) = -1$) otherwise. The total length of the time series is $L = 283041$. In this study, we considered 60 active neurons among 160 neurons to exclude silent neurons that show low firing rates for most of the time. Figure 5(a) summarizes our problem setting. We have neuronal activity recording data (top panel). After decimating 50% of them randomly (center panel), we seek to reconstruct the missing data using inference algorithms (bottom panel).

We consider three different inference methods: NEQ, NULL, and EQ. First, NEQ is the kinetic or non-equilibrium Ising model that we explained in the previous sections. Second, NULL is an unstructured model that assumes independent firing of neurons. This model restores missing data with random binary values of which mean activities are constrained to follow the data statistics. Third, EQ is the standard equilibrium Ising model that has been widely used to model collective behavior of neural networks [2, 3, 27]. This algorithm uses an EM-based approach similar to NEQ, whereas EQ considers the neural activities at different times separately (See Appendix A for the details of EQ). Note that to consider intrinsically silent neurons, NEQ and EQ include external bias b_i as well as neighboring interactions W_{ij} .

All three methods could restore the missing data (here we used $p = 0.5$). NEQ shows the highest restoration accuracy (RA = 91.1%), compared with 88.1% for NULL and 89.6% for EQ (Fig. 5(b)). However, the restoration accuracy of NEQ is not outstanding. This is because the

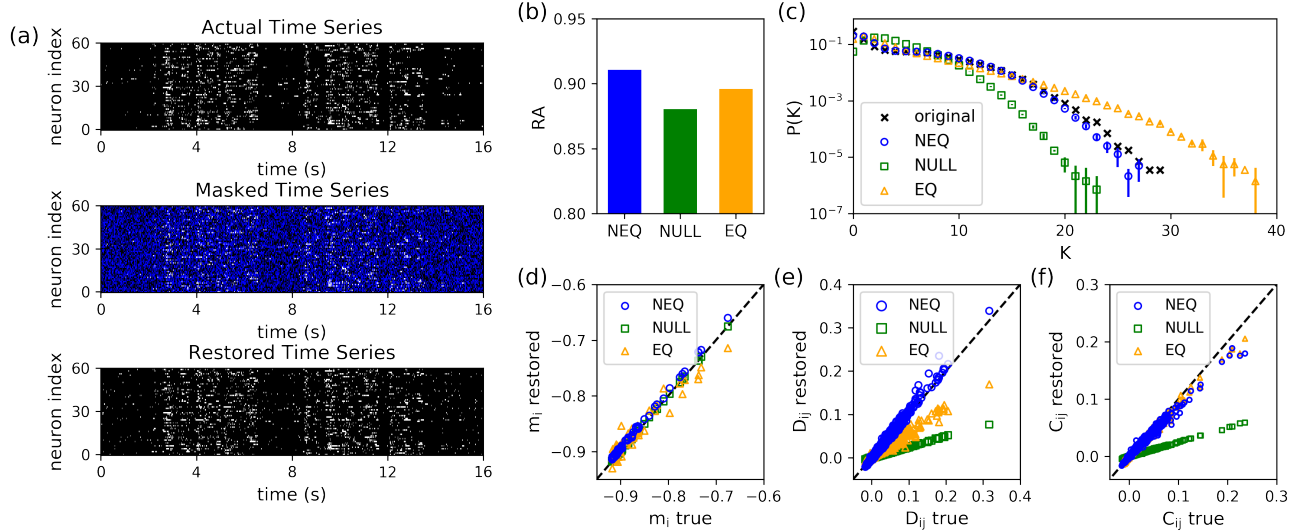


FIG. 5. Test of our algorithm on neuronal activity data published by Tkačik *et al.* [32]. (a) Raster plot of activities of 60 neurons (top). We erased the data randomly with a probability $p = 0.5$ (center), then recovered the data using our inference algorithm (bottom). (b) RA of the three data restoration algorithms based on different physical models: nonequilibrium (NEQ), independent (NULL), or equilibrium (EQ) model. Standard deviations were calculated from 5 independent trials but were negligible. (c) Inferred (blue, green, and orange) and measured (black) probability of K simultaneous spikes. (d-f) Comparison between true and restored mean activity m_i (d), one-step lagged correlation D_{ij} (e), and equal-time correlation C_{ij} (f) for the three inference algorithms.

neurons are mostly inactive (see Fig. 5(a), top panel). Indeed, if we simply assign all the missing data as *inactive* ($\sigma_i(t) = -1$), this restoration shows a better RA = 93.5% than the three methods even including NEQ. However, this naive restoration would perturb all the collective properties in data. Therefore, RA is not an appropriate estimator of the quality of data restoration. Thus we considered other descriptive statistics of the original and restored data. First, we measured the number of simultaneous spikes, $K(t) = \sum_{i=1}^N (\sigma_i(t) + 1)/2$, at different times, and obtained their relative frequencies $P(K)$ (Fig. 5(c)). Figure 5(c) clearly indicates that NEQ matches the original $P(K)$ much better than the other two methods. NULL underestimates a probability of large K s, while EQ predicts a heavier tail for $P(K)$ than the original one. These tendencies for NULL and EQ have been also observed by Tkačik *et al.* [27], where they tried to solve this issue by using an equilibrium model with pairwise interactions and an additional potential energy depending on K . Here we emphasize that NEQ, implementing non-equilibrium dynamics into the system, naturally captures the pattern of simultaneous firing without further assumptions.

Next, we examined mean activities $m_i = \langle \sigma_i(t) \rangle_t$ (Fig. 5(d)), the one-step lagged correlations $D_{ij} = \langle \sigma_i(t)\sigma_j(t+1) \rangle_t - \langle \sigma_i(t) \rangle_t \langle \sigma_j(t) \rangle_t$ (Fig. 5(e)), and the equal-time correlations $C_{ij} = \langle \sigma_i(t)\sigma_j(t) \rangle_t - \langle \sigma_i(t) \rangle_t \langle \sigma_j(t) \rangle_t$ (Fig. 5(f)). NEQ correctly infers all the statistics of m_i , C_{ij} , and D_{ij} , although it slightly underestimates C_{ij} . The correct estimation of C_{ij} is surprising because NEQ matches m_i and D_{ij} by tuning b_i and

W_{ij} [14, 15], and therefore it does not directly affect C_{ij} . Similarly, the correct estimation of m_i and C_{ij} by EQ is not surprising because EQ models m_i and C_{ij} by tuning b_i and W_{ij} . However, EQ severely underestimates D_{ij} , perhaps because neuronal firing is far from an equilibrium process in that it is a manifestation of information transmission. Finally, NULL by definition fits only m_i and obviously fails to account for pairwise correlations between spins, both C_{ij} and D_{ij} . As a further corroboration of the validity of NEQ, we examined another data set of neuronal activities [33], and confirmed that NEQ reproduces the collective behavior of neurons as shown here (see Appendix B). To sum up, these results clearly demonstrate that our algorithm (NEQ) is an effective approach for understanding real experimental data.

IV. DISCUSSION

We developed an expectation-maximization based algorithm that infers the kinetic Ising model from stochastic time series with missing data. The algorithm alternates between an E-step restoring missing data points and an M-step optimizing model parameters. We found an effective scheme for determining the optimal number of iterations that provide the best model inference. At the optimal iteration, the data-model consistency of restored data (measured by D_{mis}) is equivalent to the data-model consistency (D_{obs}) of observed data. Using the EM method with the optimal number of iterations, we could successfully infer model parameters without under-

or over-estimation even when up to 70% of the data is missing. We demonstrated the performance of the inference with synthetic data from simulations of the kinetic Ising model, and with real neuronal data. In particular, our algorithm, based on a non-equilibrium model, outperforms equilibrium models in reproducing collective behavior in neuronal activities.

Despite the good inference performance, our algorithm has plenty of room for improvement. The main drawback of our EM algorithm is that it does not converge unless sufficient amount of data is provided. As seen in Fig. 1, the data-model discrepancy D keeps decreasing with iterations even after the error of W_{ij} starts to increase. Even if we initialize the model parameters with true W_{ij} , the RMSE ends up diverging after several iterations (data not shown). This underscores the extent to which inference and prediction are different problems. Especially given a finite amount of data, over-estimation of W_{ij} can sometimes provide better prediction of observed data (or data-model consistency) and more accurate restoration of missing data. To address this issue of inference versus prediction, we introduced an effective halting scheme of $D_{\text{obs}} = D_{\text{mis}}$. Although this idea works quite well, care has to be exercised in selecting the hyperparameter ϵ that determines the inequality, $D_{\text{mis}} - D_{\text{obs}} < \epsilon$. The specific value of ϵ does not change the inference performance, if it resides within a reasonable range. Unlike the synthetic data, however, when we dealt with real data, sometimes too small ϵ could not detect the crossing of D_{obs} and D_{mis} .

This study applied the EM algorithm for the kinetic Ising model. However, other non-equilibrium models can be considered as the underlying stochastic model. For instance, Marre *et al.* [34] proposed an Ising model incorporating both spatial and temporal correlations among neurons, and showed that this model predicts spatio-temporal patterns of neuronal activities significantly better than the standard Ising model (also see [35, 36]). Moreover, Tyrcha *et al.* [37] showed that applying non-stationary external bias can explain a structure of neuronal spike trains even without direct interactions between neurons.

Our methodology to deal with incomplete kinetic Ising data can be applied to other fundamental scenarios. For example, we can apply our algorithm to data with irregular observation times. Unequally spaced time series data are common in astronomy [38, 39], paleoclimatology [40], biology [41], and many other fields in which regular observations are infeasible. In the context of the kinetic Ising model, sequences at unobserved times can be correctly inferred using exactly the same approach as this paper. Other applications would be the reconstruction of interaction networks from missing data as in [25]. Various techniques such as ℓ_1 -regularization [42] or decimation [43, 44] can be utilized with our approach as in [26]. In conclusion, we expect that our new method can be generalized for many applications.

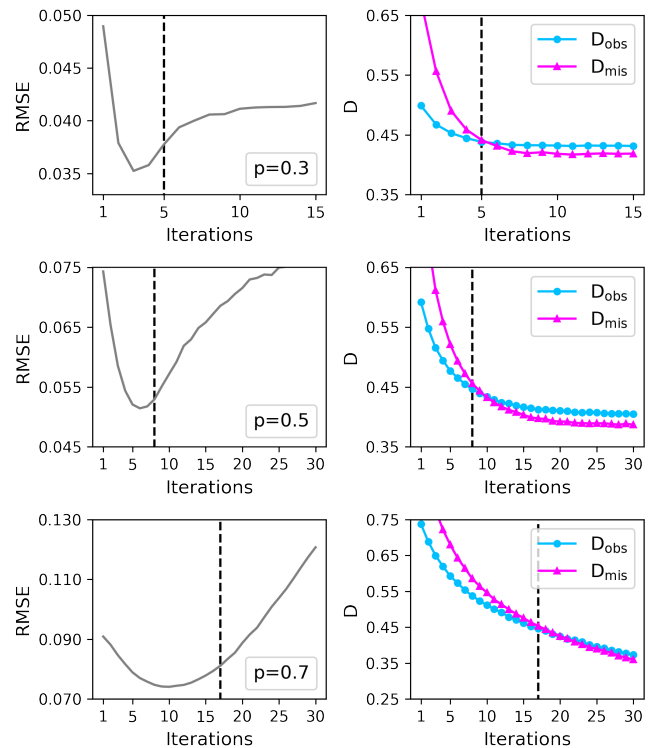


FIG. A1. The same as Fig. 1(a) but with the equilibrium Ising model.

ACKNOWLEDGMENT

This work was supported by the Intramural Research Program of the National Institutes of Health, NIDDK (V.P.), and the New Faculty Startup Fund from Seoul National University, and the National Research Foundation of Korea (NRF) grant funded by the Korea government (MSIT) (Grant No. 2019R1F1A1052916) (J.J.).

Appendix A: Equilibrium Ising Model

In this Appendix, we describe the data restoration algorithm based on the equilibrium Ising model, which we have briefly mentioned in Sec. III B. In the standard Ising model, the probability of the spin configuration $\vec{\sigma} = (\sigma_1, \sigma_2, \dots, \sigma_N)$ with $\sigma_i = \pm 1$ is expressed by the energy function $E(\vec{\sigma})$ as $P(\vec{\sigma}) = Z^{-1} \exp[-E(\vec{\sigma})]$, where $Z = \sum_{\vec{\sigma}} \exp[-E(\vec{\sigma})]$ is the normalization factor. The energy is described by $E(\vec{\sigma}) = -\sum_{i \neq j} W_{ij} \sigma_i \sigma_j - \sum_i b_i \sigma_i$, where W_{ij} is an interaction parameter and b_i an external bias. The task is to reconstruct samples and find the true W_{ij} when some portion of the the data points have not been observed.

We again split the algorithm into E- and M- steps. First, we initialize missing $\sigma_i(t)$ with random binary values (in the equilibrium model, the time index t merely acts as a label to distinguish different sequences of $\vec{\sigma}$).

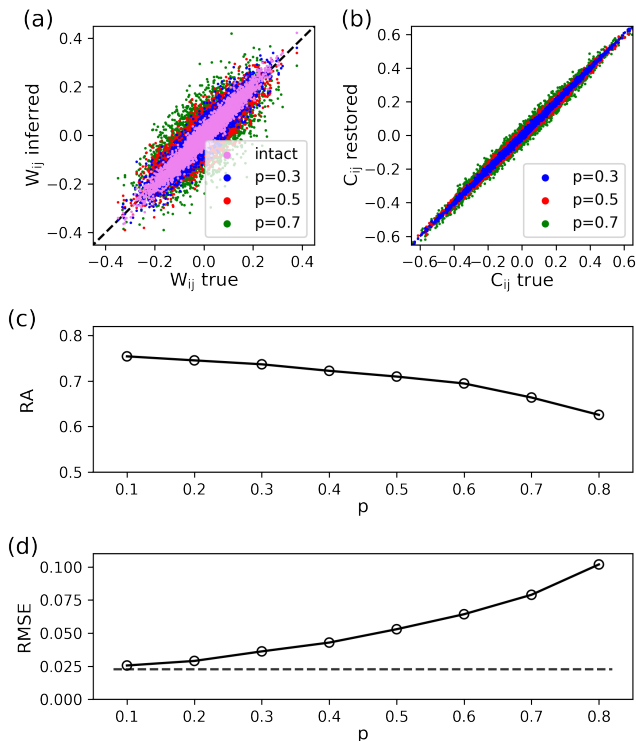


FIG. A2. The same as Fig. 2 but with the equilibrium Ising model. Also, the one-step lagged correlation D_{ij} in Fig. 2(b) is replaced by the equal-time correlation C_{ij} .

From the randomly assigned data, we find an error-prone W_{ij} (see below). Then it is reasonable to mimic the Metropolis-Hastings algorithm [45] to update missing data points (E-step). Indeed, at each turn, we choose to flip or not to flip $\sigma_i(t)$ using the ratio of two probabilities $P(F_i(\vec{\sigma}(t)))/P(\vec{\sigma}(t))$, where $F_i(\vec{\sigma}(t)) = (\sigma_1(t), \dots, -\sigma_i(t), \dots, \sigma_N(t))$. As in the main text, we updated all of the missing data one by one for each t . We checked that increasing the number of updates in one step did not affect the results.

Given the reconstructed samples, we can infer the best W_{ij} (M-step) by maximizing the data likelihood called the Boltzmann machine [46]. However, this requires an extensive calculation of the normalization factor Z , which entails the sum of 2^N configurations. Physicists have developed a number of methods to circumvent the exact computation of Z , including mean-field [47, 48], Bethe approximation [49], Sessak-Monasson [50], and adaptive cluster expansions [51] (see also a pedagogical review [16]). In this study, we chose a maximum pseudo-likelihood approach [52] that maximizes the *local* pseudo-likelihood of $\mathcal{L}_i = \prod_t P(\sigma_i(t) | \vec{\sigma}_i^c(t))$ for each i , where $\vec{\sigma}_i^c$ denotes all spins besides the i -th spin. Since $P(\sigma_i(t) | \vec{\sigma}_i^c(t))$ is determined by a local field $H_i(t) =$

$\sum_{j \neq i} W_{ij} \sigma_j(t) + b_i$, the same logistic regression function [30] can be utilized, allowing fast and accurate inference. After optimizing each \mathcal{L}_i separately, we set $W_{ij} \leftarrow (W_{ij} + W_{ji})/2$ to ensure symmetric couplings.

Running this algorithm, we found the evidence of overfitting similarly observed in Fig. 1. To avoid overfitting, we defined the same data-model discrepancy as Eq. 5 for observed and missing data (D_{obs} and D_{mis}) with the replacement of $\sigma_i(t+1)$ to $\sigma_i(t)$. We tracked the evolution of D_{obs} and D_{mis} and halted the algorithm when the stopping condition $D_{\text{mis}} - D_{\text{obs}} < \epsilon$ is satisfied (we again set $\epsilon = 0.01$). Overall, the algorithm with the equilibrium Ising model (EQ) is nearly the same as the one with the kinetic Ising model (NEQ) in the main text. The main differences are (i) we use the Metropolis-Hastings based approach to assign missing data and (ii) we use the local pseudo-likelihood maximization to infer W_{ij} .

Figure A1 illustrates our stopping criterion for EQ. Samples were generated using the Metropolis-Hastings algorithm with a system size $N = 100$ and a sample size $L = 10000$. We found that the algorithm stops several steps after reaching the minimum error of W_{ij} , which means that the inference of W_{ij} is suboptimal. This is different from the case of NEQ where we could see the coincidence between the minimum of RMSE (Fig. 1, left panels) and the intersection of D_{obs} and D_{mis} (right panels). Even with this perhaps improper stopping condition, we observed that the algorithm is capable of inferring the true W_{ij} even with a fraction of missing data as large as $p = 0.7$ (Fig. A2(a)). Furthermore, an excellent agreement between the pair correlations C_{ij} of the true and restored data was found (Fig. A2(b)), in contrast to the relatively large deviation of the inferred W_{ij} .

To address the quality of data restoration, we defined restoration accuracy (RA) the same as in the main text. Figure A2(c) shows that RA is above 0.6 even when 80% of the data have been decimated. Figure A2(d) displays a similar behavior to Fig. 2(d). Predictably, the quality of the inference gradually decreases with p . When p is smaller than 0.4, we can obtain W_{ij} with an error less than 5%.

Appendix B: Other Experimental Data

In addition to Sec. III B, we tested our algorithms with other neuronal spike train data published by Kohn and Smith [33]. They recorded spiking activities of 70-100 neurons in the visual cortex of adult monkeys under various visual stimuli. Here, we chose a ‘‘spontaneous’’ dataset where a uniform gray screen had been used. We binned the neural activity with 20 ms and selected the most active 60 neurons. The data length was $L = 123404$. For the detailed experimental procedure, see [53, 54]. We summarize the results in Fig. A3 with the same format as Fig. 5. The results are similar.

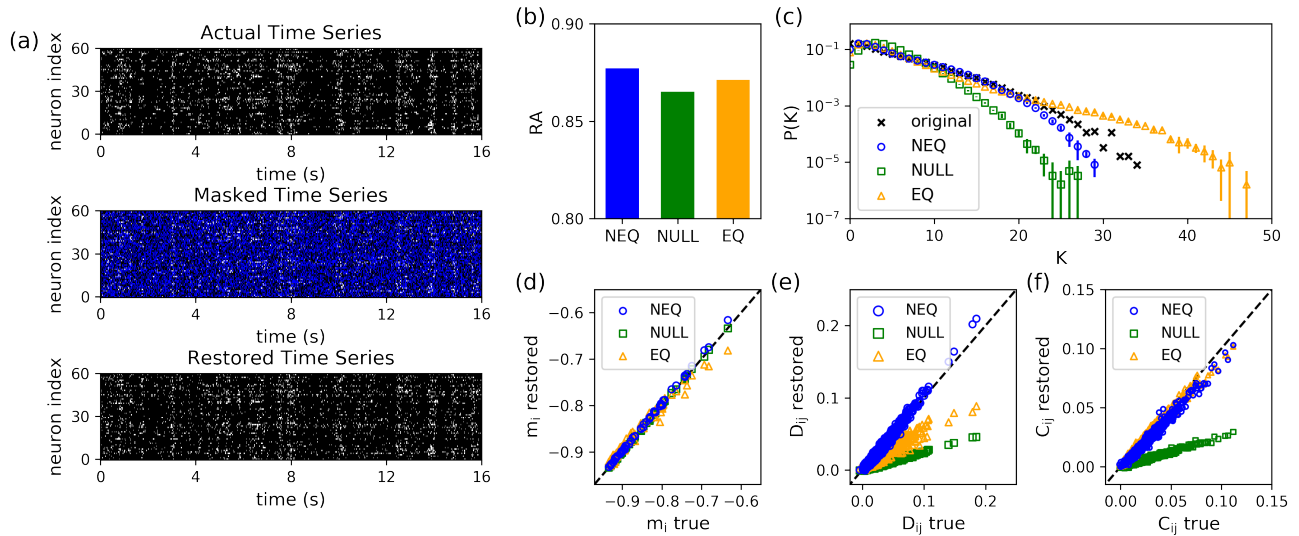


FIG. A3. The same as Fig. 5 but using neuronal activity data published by Kohn and Smith [33].

-
- [1] S. Brunton and N. Kutz, *Data-driven science and engineering: machine learning, dynamical systems, and control* (Cambridge University Press, Cambridge, England, UK, 2019).
- [2] E. Schneidman, I. I. Michael J. Berry, R. Segev, and W. Bialek, *Nature* **440**, 1007 (2006).
- [3] J. Shlens, G. D. Field, J. L. Gauthier, M. I. Grivich, D. Petrusca, A. Sher, A. M. Litke, and E. J. Chichilnisky, *J. Neurosci.* **26**, 8254 (2006).
- [4] A. Lapedes, B. Giraud, and C. Jarzynski, arXiv (2012), 1207.2484.
- [5] F. Morcos, A. Pagnani, B. Lunt, A. Bertolino, D. S. Marks, C. Sander, R. Zecchina, J. N. Onuchic, T. Hwa, and M. Weigt, *Proc. Natl. Acad. Sci. U.S.A.* **108**, E1293 (2011).
- [6] T. Mora, A. M. Walczak, W. Bialek, and C. G. Callan, Jr., *Proc. Natl. Acad. Sci. U.S.A.* **107**, 5405 (2010).
- [7] T. R. Lezon, J. R. Banavar, M. Cieplak, A. Maritan, and N. V. Fedoroff, *Proc. Natl. Acad. Sci. U.S.A.* **103**, 19033 (2006).
- [8] T. Bury, *Physica A* **392**, 1375 (2013).
- [9] Y. Shemesh, Y. Sztainberg, O. Forkosh, T. Shlapobersky, A. Chen, and E. Schneidman, *eLife* (2013), 10.7554/eLife.00759.
- [10] E. D. Lee, C. P. Broedersz, and W. Bialek, *J. Stat. Phys.* **160**, 275 (2015).
- [11] M. Figliuzzi, P. Barrat-Charlaix, and M. Weigt, *Mol. Biol. Evol.* **35**, 1018 (2018).
- [12] Y. Roudi, S. Nirenberg, and P. E. Latham, *PLoS Comput. Biol.* **5**, e1000380 (2009).
- [13] B. Derrida, E. Gardner, and A. Zippelius, *EPL* **4**, 167 (1987).
- [14] Y. Roudi and J. Hertz, *Phys. Rev. Lett.* **106**, 048702 (2011).
- [15] H.-L. Zeng, M. Alava, E. Aurell, J. Hertz, and Y. Roudi, *Phys. Rev. Lett.* **110**, 210601 (2013).
- [16] H. C. Nguyen, R. Zecchina, and J. Berg, *Adv. Phys.* **66**, 197 (2017).
- [17] M. Mézard and J. Sakellariou, *J. Stat. Mech.: Theory Exp.* **2011**, L07001 (2011).
- [18] D.-T. Hoang, J. Song, V. Periwal, and J. Jo, *Phys. Rev. E* **99**, 023311 (2019).
- [19] B. Dunn and Y. Roudi, *Phys. Rev. E* **87**, 022127 (2013).
- [20] J. Tyrcha and J. Hertz, *Mathematical Biosciences & Engineering* **11**, 149 (2014).
- [21] L. Bachschmid-Romano and M. Opper, *J. Stat. Mech.: Theory Exp.* **2014**, P06013 (2014).
- [22] C. Battistin, J. Hertz, J. Tyrcha, and Y. Roudi, *J. Stat. Mech.: Theory Exp.* **2015**, P05021 (2015).
- [23] D.-T. Hoang, J. Jo, and V. Periwal, *Phys. Rev. E* **99**, 042114 (2019).
- [24] A. P. Dempster, N. M. Laird, and D. B. Rubin, *Journal of the Royal Statistical Society: Series B (Methodological)* **39**, 1 (1977).
- [25] D. Soudry, S. Keshri, P. Stinson, M.-h. Oh, G. Iyengar, and L. Paninski, *PLoS Comput. Biol.* **11**, e1004464 (2015).
- [26] C. Campajola, F. Lillo, and D. Tantari, *Phys. Rev. E* **99**, 062138 (2019).
- [27] G. Tkačik, O. Marre, D. Amodei, E. Schneidman, W. Bialek, and M. J. B. I. I., *PLoS Comput. Biol.* **10**, e1003408 (2014).
- [28] X. Chen, F. Randi, A. M. Leifer, and W. Bialek, *Phys. Rev. E* **99**, 052418 (2019).
- [29] H.-L. Zeng, E. Aurell, M. Alava, and H. Mahmoudi, *Phys. Rev. E* **83**, 041135 (2011).
- [30] F. Pedregosa, G. Varoquaux, A. Gramfort, V. Michel, B. Thirion, O. Grisel, M. Blondel, P. Prettenhofer, R. Weiss, V. Dubourg, J. Vanderplas, A. Passos, D. Cournapeau, M. Brucher, M. Perrot, and E. Duchesnay, *Journal of Machine Learning Research* **12**, 2825 (2011).
- [31] D. Sherrington and S. Kirkpatrick, *Phys. Rev. Lett.* **35**, 1792 (1975).

- [32] O. Marre, G. Tkacik, D. Amodei, E. Schneidman, W. Bialek, and M. Berry, *Multi-electrode array recording from salamander retinal ganglion cells*, IST Austria (2017).
- [33] A. Kohn and M. A. Smith, *Utah array extracellular recordings of spontaneous and visually evoked activity from anesthetized macaque primary visual cortex (V1)*, CRCNS.org (2016).
- [34] O. Marre, S. El Boustani, Y. Frégnac, and A. Destexhe, *Phys. Rev. Lett.* **102**, 138101 (2009).
- [35] H. Nasser, O. Marre, and B. Cessac, *J. Stat. Mech.: Theory Exp.* **2013**, P03006 (2013).
- [36] H. Nasser and B. Cessac, *Entropy* **16**, 2244 (2014).
- [37] J. Tyrcha, Y. Roudi, M. Marsili, and J. Hertz, *J. Stat. Mech.: Theory Exp.* **2013**, P03005 (2013).
- [38] N. R. Lomb, *Astrophys. Space Sci.* **39**, 447 (1976).
- [39] J. D. Scargle, *Astrophys. J.* **263**, 835 (1982).
- [40] M. Schulz and M. Mudelsee, *Comput. Geosci.* **28**, 421 (2002).
- [41] T. Ruf, *Biol. Rhythm Res.* **30**, 178 (1999).
- [42] P. Ravikumar, M. J. Wainwright, and J. D. Lafferty, *Ann. Stat.* **38**, 1287 (2010).
- [43] A. Decelle and F. Ricci-Tersenghi, *Phys. Rev. Lett.* **112**, 070603 (2014).
- [44] A. Decelle and P. Zhang, *Phys. Rev. E* **91**, 052136 (2015).
- [45] W. K. Hastings, *Biometrika* **57**, 97 (1970).
- [46] D. H. Ackley, G. E. Hinton, and T. J. Sejnowski, *Cognitive Science* **9**, 147 (1985).
- [47] H. Kappen, F. Rodríguez, and F. B. Rodríguez, in *Advances in Neural Information Processing Systems* (The MIT Press, 1998) pp. 280–286.
- [48] T. Tanaka, *Phys. Rev. E* **58**, 2302 (1998).
- [49] F. Ricci-Tersenghi, *J. Stat. Mech.: Theory Exp.* **2012**, P08015 (2012).
- [50] V. Sessak and R. Monasson, *J. Phys. A: Math. Theor.* **42**, 055001 (2009).
- [51] J. P. Barton, E. De Leonardis, A. Coucke, and S. Cocco, *Bioinformatics* **32**, 3089 (2016).
- [52] E. Aurell and M. Ekeberg, *Phys. Rev. Lett.* **108**, 090201 (2012).
- [53] M. A. Smith and A. Kohn, *J. Neurosci.* **28**, 12591 (2008).
- [54] R. C. Kelly, M. A. Smith, R. E. Kass, and T. S. Lee, *J. Comput. Neurosci.* **29**, 567 (2010).